

## Electromagnetic-Wave Tunneling Through Negative-Permittivity Media with High Magnetic Fields

Lei Zhou,<sup>1,2,\*</sup> Weijia Wen,<sup>1</sup> C. T. Chan,<sup>1</sup> and Ping Sheng<sup>1</sup>

<sup>1</sup>Department of Physics, Hong Kong University of Science and Technology, Clear Water Bay, Kowloon, Hong Kong, China

<sup>2</sup>Surface Physics Laboratory (State Key Laboratory) and Physics Department, Fudan University, Shanghai 200433, China

(Received 22 November 2004; published 24 June 2005)

We demonstrate that electromagnetic waves can transmit *with unit transmittance* through a slab of negative-permittivity media sandwiched between two identical slabs with high permittivity, although each single slab is nearly opaque. This type of transparency is accompanied by high magnetic fields, and is robust against incidence angles. Microwave experiments, in excellent agreement with finite-difference-time-domain simulations, are performed to successfully realize this idea.

DOI: 10.1103/PhysRevLett.94.243905

PACS numbers: 42.25.Bs, 41.20.Jb, 78.20.-e

Induced high transmittance of electromagnetic (EM) waves through opaque media has always been fascinating. Such a phenomenon is typically associated with the excitation of some kind of resonances. For example, the excitation of surface plasmons (SP's) [1], say using prism couplers, can induce high transmission through an opaque metallic film [2]. Excitation of SP's can also be enabled by the Bragg scattering of periodical surface structures, which explains Ebessen *et al.*'s experiment of high transmissions [3] through metal films with an array of subwavelength air holes [4–8]. High transmission through metallic films with thin slits can also be induced by Fabry-Perot (FP) resonance of *propagating* waves inside the slits [9–11]. We propose here another mechanism, different from the SP-aided [2–8] and FP ones [9–11], to make a classically opaque flat slab with a negative  $\varepsilon$  (*allowing evanescent waves only*) perfectly transparent. We will discuss the conditions to realize this phenomenon and the associated unusual characteristics. Specifically, we show the perfect transparency to be accompanied by high magnetic fields at interfaces, and robust against varying incidence angles. We have performed microwave experiments and finite-difference-time-domain (FDTD) simulations [12] to successfully realize this idea.

While our idea is motivated by effective medium theory (EMT), the final conclusion is drawn from measurements of real samples and FDTD simulations. Let us consider a homogeneous layer *B* of thickness  $d_2$  with  $\varepsilon_2 < 0$ , which by itself is opaque. Consider first a double layer structure combining this layer with another homogeneous layer *A* with  $\varepsilon_1 > 0$  and thickness  $d_1$ . Within the effective medium framework, the *AB* structure will become transparent when  $\bar{\varepsilon} = (\varepsilon_1 d_1 + \varepsilon_2 d_2)/(d_1 + d_2) = 1$ . For a circular frequency  $\omega$  and fixed parallel  $\mathbf{k}$  component  $k_{\parallel}$ , we obtain a  $2 \times 2$  transfer matrix  $Q(\omega, k_{\parallel})$ , by which both the transmission coefficient  $t = Q_{11} - Q_{12}Q_{21}/Q_{22}$  and reflection coefficient  $r = -Q_{21}/Q_{22}$  can be calculated [13]. If there is no absorption, perfect transmission ( $T = |t|^2 = 1$ ) appears when  $Q_{21} = 0$ . For this *AB* structure, the criterion of

perfect transmission at normal incidence ( $k_{\parallel} = 0$ ) is

$$\left(\frac{k_1}{k_0} - \frac{k_0}{k_1}\right) \tan(k_1 d_1) - \left(\frac{\alpha_2}{k_0} + \frac{k_0}{\alpha_2}\right) \tanh(\alpha_2 d_2) + i\left(\frac{k_1}{\alpha_2} + \frac{\alpha_2}{k_1}\right) \tan(k_1 d_1) \tanh(\alpha_2 d_2) = 0, \quad (1)$$

where  $k_l = \sqrt{\varepsilon_l} \frac{\omega}{c}$  and  $k_2 = i\alpha_2$ . Since the first two terms are real while the third term is imaginary, Eq. (1) can *never* be satisfied, indicating that *perfect* transmission cannot be realized in the *AB* structure. The reason is that the waves scattered by layers *A* and *B* cannot *completely* cancel each other, since the two layers are in different phase planes. This problem can be remedied when another identical *A* layer is added to form an *ABA* sandwich structure. For this structure, we find the following *rigorous* criterion for perfect transmission:

$$\left(\frac{k_1}{k_0} - \frac{k_0}{k_1}\right) 2 \tan(k_1 d_1) - \left(\frac{\alpha_2}{k_0} + \frac{k_0}{\alpha_2}\right) \tanh(\alpha_2 d_2) - \left(\frac{k_1^2}{\alpha_2 k_0} + \frac{\alpha_2 k_0}{k_1^2}\right) \tan^2(k_1 d_1) \tanh(\alpha_2 d_2) = 0. \quad (2)$$

The third term in the above equation is also real so that Eq. (2) *can* be satisfied with appropriate parameter values. This perfect transmission is not induced by SP's, since the latter correspond to the condition  $Q_{22}(\omega, k_{\parallel}) = 0$  [14], while the present criterion is  $Q_{21}(\omega, k_{\parallel}) = 0$ . The present transparency is also not induced by FP interference [9–11], since no propagating wave is allowed inside our *B* layer.

The first two terms in Eq. (2) are single scattering contributions of individual *A* and *B* layers, while the third term is a multiple scattering contribution. In the long-wavelength limit ( $k_i d_i \rightarrow 0$ ), the third term can be dropped and Eq. (2) is reduced to the EMT solution:  $\bar{\varepsilon} = (2\varepsilon_1 d_1 + \varepsilon_2 d_2)/(2d_1 + d_2) = 1$ . However, when  $k_1 d_1$  and  $\alpha_2 d_2$  are *not* small, Eq. (2) still has solutions. Figure 1(a) shows the solved values of  $\varepsilon_1$  as a function of  $d_2$  for an example with  $\varepsilon_2 = -2000$ . To avoid the confusion of too many parameters, we set  $d_1 = d_2 = d$ . We find the existence of two

solutions up to a critical thickness at which the solutions merge together and disappear abruptly. The first solution recovers the EMT value in the limit of  $k_0d \rightarrow 0$ , but at the critical thickness, we have  $k_1d \approx 1.3$ ,  $\alpha_2d \approx 2.7$ , far away from the long-wavelength limit requirement. The first solution deviates from the EMT value with increasing  $d$ , although it is derived from the EMT. A  $\varepsilon_2 \sim d$  phase diagram is shown in Fig. 1(b) for this EMT-derived solution  $\varepsilon_1$ , scaled by its corresponding EMT value. A phase boundary is found to separate the lower-left region which supports the  $T = 1$  solutions from the upper-right one which does not. The solution is closer to the EMT value in regions closer to the lower-left corner where EMT is better applicable. However,  $T = 1$  solutions survive when EMT is apparently no longer valid.

Figs. 2(a) and 2(b) show the field patterns for the two  $T = 1$  solutions. In both cases, we find exponentially growing evanescent waves inside the  $B$  layer to *completely* compensate the usual exponentially decaying wave, resulting in perfect transmissions. We find the magnetic fields to be strongly enhanced around the  $A$ - $B$  interfaces, which is a characteristic feature of this phenomenon but not found in others [2–11]. On the other hand, the electric field is diminished inside the  $B$  layer. After considering the phase (not shown here), we find the magnetic field pattern to exhibit odd symmetry with respect to the center plane of layer  $B$  for the EMT-derived solution, and even symmetry for the second solution. A phase diagram is given in Fig. 2(c) to show the maximum enhancement of magnetic field with respect to parameters  $\varepsilon_2$  and  $d$  ( $= d_1 = d_2$ ) for the EMT-derived transmission. The field enhancement is stronger with larger  $\varepsilon_2$  and appropriate  $d$ , in clear contrast to the EMT applicable region shown in Fig. 1(b). This indicates that the high magnetic field is *not* a natural consequence of EMT.

We perform experiments in the microwave regime and FDTD simulations [15] to demonstrate such an effect. In order to realize materials with negative  $\varepsilon$  or large positive  $\varepsilon$  in the microwave regime, we use resonance structures, in the same spirit as “metamaterials,” in which a wide range of effective  $\varepsilon$  is achieved with subwavelength microstruc-

tures [16]. To realize the “ $B$ ” layer with a negative effective  $\varepsilon$ , we fabricated a 0.1 mm-thick metallic mesh with periodically arranged  $3.5 \text{ mm} \times 3.5 \text{ mm}$  air squares with a lattice constant of 4.0 mm. The metallic mesh was sandwiched between two 0.35 mm-thick substrates ( $\varepsilon_{\text{sub}} = 6.5$ ) to ensure the symmetry requirement. The measured transmission spectrum [17] within 1–10 GHz for this  $B$  layer is shown in Fig. 3(a), compared with the FDTD results. Both experiments and FDTD show that the transmittance is very low in this frequency regime, since the air square size is at least 10 times smaller than wavelength [18]. Transmission through this  $B$  layer can be modeled by treating the layer as a homogeneous slab (of the same thickness 0.8 mm) with  $\varepsilon_2 = 6.5 - 62^2/f^2$ . Using such a model, both the transmittance [shown in Fig. 3(a)] and the transmission phase can be accurately reproduced [19]. We employ the resonance principle to construct our layer  $A$  with required high  $\varepsilon$ . The metallic structure shown in the inset to Fig. 3(b) is replicated in the  $xy$  plane with a lattice constant = 12 mm. The resulting periodic planar structure was deposited on a 1.6 mm-thick dielectric substrate (with  $\varepsilon_{\text{sub}} = 4$ ) to form our layer  $A$ . From the measured normal transmission spectrum shown in Fig. 3(b), which is in excellent agreement with the FDTD results, we find a clear dip in 4.59 GHz,

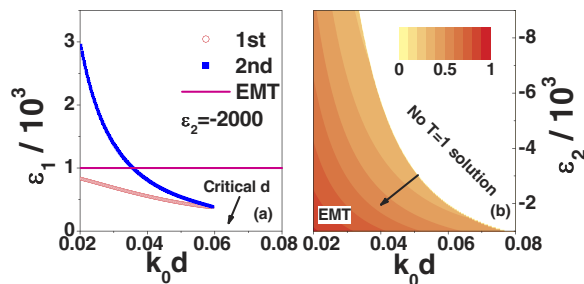


FIG. 1 (color online). (a)  $\varepsilon_1$  satisfying Eq. (2) as functions of  $d$ . Horizontal (magenta online) line denotes the EMT solution  $\varepsilon_{\text{EMT}} = 3/2 - \varepsilon_2/2$ . (b)  $\varepsilon_2 \sim d$  phase diagram depicting the value of  $\varepsilon_1/\varepsilon_{\text{EMT}}$  for the EMT-derived perfect transmission solution.

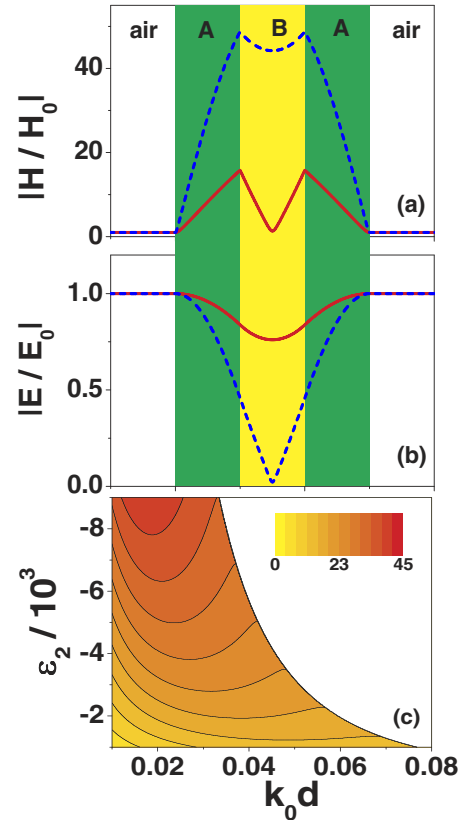


FIG. 2 (color online).  $|H/H_0|$  (a) and  $|E/E_0|$  (b) as the functions of position for the EMT-derived solution (solid line) and the other solution (dashed line). Here  $\varepsilon_2 = -2000$ ,  $k_0d = 0.02$ . (c) Maximum magnetic field enhancement obtained in the EMT-derived perfect transmission state with respect to  $\varepsilon_2$  and  $d$ .

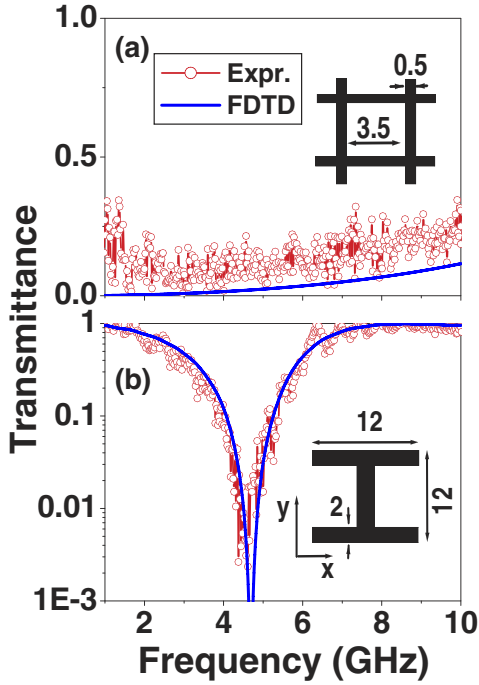


FIG. 3 (color online). Measured (circles) and calculated (lines) transmission spectra of a single metallic mesh layer (a), and a single metallic resonance layer (b). The metallic structures are shown in the insets with all lengths measured in mm.

corresponding precisely to the resonance frequency. Again, if we model the layer *A* by a homogeneous 1.65 mm-thick slab with  $\epsilon_1 = 4.0 + 200/(4.59^2 - f^2)$ , both the transmittance [Fig. 3(b)] and the transmission phase can be well reproduced [19].

We now study the *ABA* structure. A series of measurements and simulations were performed on such systems with different air gaps to separate layers *A* and *B* [see the inset to Fig. 4(a)]. When the gap is very small, FDTD simulations [lines in Fig. 4(a)] show two perfect transmission peaks at about 3.15 and 3.83 GHz. These two peaks correspond precisely to the two perfect transmission solutions shown in Fig. 1(a). At other frequencies, Eq. (2) cannot be satisfied, leading to strong reflections. We note from Figs. 3(a) and 3(b) that neither layers *A* nor *B* is transparent within 3–4 GHz, yet the combination of these opaque layers can lead to perfect transparency. When the gap becomes larger, the two peaks persist until a critical thickness (a little bit larger than 2 mm) is reached when they merge together [Fig. 4(b)]. If the gap is bigger than the critical thickness, no perfect transmission exists and the maximum transmittance is less than unity [Fig. 4(c)]. The physics of the critical thickness is essentially the same as that shown in Fig. 1, based on analytical calculations.

Experimental results are shown in the same figure as open circles. The overall agreement between experiments and theory is quite good for all three cases. In particular, near the critical thickness, experiments do show  $\sim 100\%$  transmissions at the frequency predicted by the theory. In each case, the experimentally measured transmission is

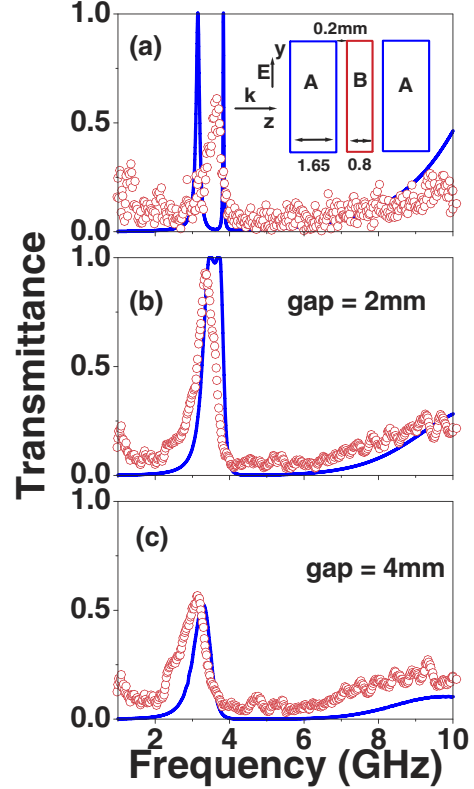


FIG. 4 (color online). Measured (circles) and calculated (lines) transmission spectra of the *ABA* structure with different air gaps between layers *A* and *B*.

substantially higher than that for a single mesh layer [Fig. 3(a)]. However, for the case of very small gap, the experimental peak is much broader than theoretical predictions and there is only one main peak instead of two, probably due to finite-size effects and absorptions.

We discuss two properties related to this transparency. FDTD simulations verified the high magnetic field associated with this transparency. For the system with a 2 mm-thick gap, we find the magnetic field to be strongly enhanced in a wide frequency band (3.4–3.8 GHz) where the transmittance is  $\sim 100\%$ . Figure 5(a) shows the local magnetic field distribution on the *xy* plane located in the air gap between layers *A* and *B* at a particular frequency  $f = 3.8$  GHz. In the case of a smaller air gap, the field enhancement is even larger at the expense of a narrower frequency range.

Another property is the angle-independence of the high transmission. Figure 5(b) depicts the FDTD-calculated perfect transmission frequencies as functions of the incidence angle for the *S*-polarized incidence wave (i.e., keeping  $\vec{E} \parallel \hat{y}$ , see inset to Fig. 4(a)) [20], again for the 2 mm-gap system. The perfect transmissions are stable against varying incidence angle up to very large values. This is quite different from the SP-aided high transmissions, which strongly depend on incidence angles [2,3]. The stability is understood by examining Eq. (2), in which  $k_l$  should be substituted by  $k_l^z$  in the oblique angle case. Under an

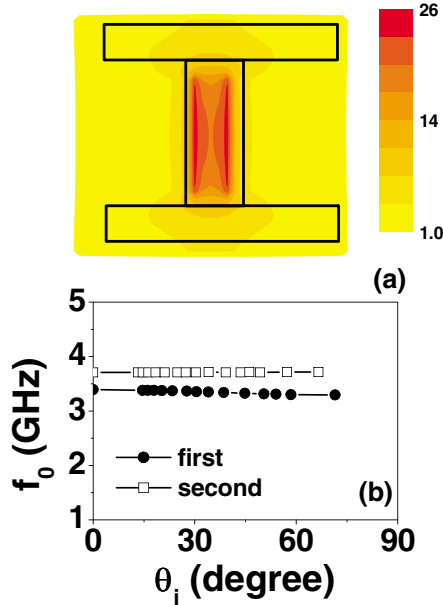


FIG. 5 (color online). (a) Distribution of local magnetic field enhancement  $|H_x(x, y)/H_x^0|$  on a  $xy$  plane located at the air gap between layers  $A$  and  $B$ , for the 2 mm-gap  $ABA$  structure. The projected position of the metallic structure in layer  $A$  is indicated. (b) Two perfect transmission frequencies  $f_0$  as functions of incidence angle  $\theta_i$  calculated by FDTD simulations for the  $ABA$  structure with a 2 mm air gap.

incidence angle  $\theta_i$  implying a fixed parallel  $k$  component  $k_i^{\parallel} = (\omega/c) \sin\theta_i$ , we have  $k_i^z = \sqrt{\epsilon_l(\omega/c)^2 - (k_i^{\parallel})^2} = \sqrt{\epsilon_l - \sin^2\theta_i}(\omega/c)$ . Since  $|\epsilon_l| \gg 1$  here, the solution of Eq. (2) has very little dependence on  $\theta_i$ , resulting in the robustness of present high transmission against incidence angles.

We note that a parallel-plate resonance cavity [21] also supports frequency-selective high transmission accompanied by high magnetic field and robust against incidence angles, *as long as the medium filling the cavity has a very large positive  $\epsilon$* . However, the high transmission through a cavity is governed by the constructive interferences of multiply scattered waves (*positive  $\epsilon$  required*), which is different from the EMT-derived mechanism for the present  $ABA$  case, in which the inside medium (i.e., the  $B$  layer) has a *negative  $\epsilon$* . Also, in the cavity case, the  $E$  field is enhanced inside the cavity and is a maximum in the cavity center, which is in sharp contrast to the patterns shown in Fig. 2(b) for the  $ABA$  case, in which the  $E$  field is suppressed and  $B$  field enhanced. Finally, we cannot find a similar critical thickness (like that in Fig. 4) for the high transmission through a resonance cavity.

In conclusion, through analytic analysis, FDTD simulations and microwave experiments, we have demonstrated a mechanism for EM wave tunneling through a classically opaque material with negative permittivity. The present

transparency is characterized by high magnetic field (in the microwave frequency regime) and is robust against varying incidence angles. The present effect is also realizable in infrared or optical regimes with appropriate designs.

This work was supported by Hong Kong RGC through CA02/03.SC01, National Basic Research Program of China (No. 2004CB719800) and PCSIRT.

\*Electronic address: phzhou@fudan.edu.cn

- [1] See, for example, *Electromagnetic Surface Modes*, edited by A. D. Boardman (John Wiley & Sons, Belfast, Northern Ireland, 1982).
- [2] R. Dragila, B. Luther-Daviers, and S. Vukovic, *Phys. Rev. Lett.* **55**, 1117 (1985).
- [3] T. W. Ebbesen *et al.*, *Nature (London)* **391**, 667 (1998).
- [4] H. F. Ghaemi *et al.*, *Phys. Rev. B* **58**, 6779 (1998).
- [5] L. Martin-Moreno *et al.*, *Phys. Rev. Lett.* **86**, 1114 (2001).
- [6] W. C. Tam, T. W. Preist, and R. J. Sambles, *Phys. Rev. B* **62**, 11134 (2000).
- [7] W. C. Liu and D. P. Tsai, *Phys. Rev. B* **65**, 155423 (2002).
- [8] L. Salomon *et al.*, *Phys. Rev. Lett.* **86**, 1110 (2001).
- [9] J. A. Porto, F. J. Garcia-Vidal, and J. B. Pendry, *Phys. Rev. Lett.* **83**, 2845 (1999).
- [10] Y. Takakura, *Phys. Rev. Lett.* **86**, 5601 (2001).
- [11] F. Yang and J. R. Sambles, *Phys. Rev. Lett.* **89**, 063901 (2002).
- [12] K. S. Yee, *IEEE Trans. Antennas Propag.* **14**, 302 (1966).
- [13] See, e.g., K. Busch, C. T. Chan, and C. M. Soukoulis, in *Photonic Band Gap Materials*, edited by C. M. Soukoulis (Kluwer, Dordrecht, 1996).
- [14] L. Zhou and C. T. Chan, *Appl. Phys. Lett.* **84**, 1444 (2004).
- [15] Simulations were performed using the package CONCERTO 3.1, developed by Vector Fields Limited, England, 2002. We adopted perfect metal boundary conditions for metal surfaces, good for microwave regime. The convergence against mesh size was carefully tested.
- [16] W. J. Wen *et al.*, *Phys. Rev. Lett.* **89**, 223901 (2002); J. P. Pendry *et al.*, *Phys. Rev. Lett.* **76**, 4773 (1996).
- [17] All microwave spectra were measured by an Agilent network analyzer. Two identical microwave horns were used to generate and receive the signals separated by a distance of 100 cm. The sample was placed on a stage, 15 cm from the receiving horn. The transmittance is normalized to that without the slab.
- [18] The strong oscillations in experimental results are induced by the finite-size effect. The finite-size effect is also partly responsible for the discrepancy with FDTD results obtained for infinite systems.
- [19] The phase information is needed to differentiate a material with  $[\epsilon, \mu]$  from its counterpart material with  $[\epsilon' \rightarrow \mu, \mu' \rightarrow \epsilon]$ .
- [20] L. Zhou, C. T. Chan, and P. Sheng, *J. Phys. D* **37**, 368 (2004); *Phys. Rev. B* **68**, 115424 (2003).
- [21] See, for example, J. D. Jackson, *Classical Electrodynamics* (Wiley, New York, 1975).